Solubility versus Electrostatics: What Determines Lipid/Protein Interaction in Lung Surfactant

M. Seifert,* D. Breitenstein,† U. Klenz,* M. C. Meyer,* and H.-J. Galla*
*Institute of Biochemistry and †Tascon GmbH, 48149 Münster, Germany

ABSTRACT Mammalian lung surfactant is a complex lipid/protein mixture covering the alveolar interface and has the crucial function of reducing the surface tension at this boundary to minimal values. Surfactant protein SP-B plays an important role for this purpose and was the focus of many recent studies. However, the specificity of lipid/SP-B interactions is controversial. Since these investigations were accomplished at varying pH conditions (pH 5.5 and 7.0), we studied the specificity of these interactions in a dipalmitoylphosphatidylcholine (DPPC)/dipalmitoylphosphatidylglycerol (DPPG)/SP-B (4:1:0.2 mol %) model system at either pH. Mainly fluorescence microscopy and laterally resolved time-of-flight secondary ion mass spectrometry were used to reveal information about the phase behavior of the lipids and the molecular distribution of SP-B in the lipid mixture. DPPG forms separated condensed domains due to a strong hydrogen-bond network, from which the protein is mainly excluded. Considering the protein as an impurity of the lipid mixture leads to the principle of the zone melting process: an impurity is highly more soluble in a liquid phase than in a solid phase. The phase behavior effect of the lipids mainly outperforms the electrostatic interactions between DPPG and SP-B, leading to a more passively achieved colocalization of DPPC and SP-B.

INTRODUCTION

Pulmonary surfactant is a lipid/protein composite that covers the air/water interface in vertebrate lungs. In this interface, lipid monolayer regions most likely coexist with surfactant protein containing multi-layer structures (1,2). Its essential function during the breathing process is the reduction of surface tension to prevent a collapse of the alveolar system during expiration and to reduce the work of breathing (3).

Malfunction or lack of this crucial material leads to diseases like neonatal respiratory distress syndrome, which is demonstrated by insufficient respiration aptitude, and without immediate medical treatment results in severe consequences or even death of the concerned individual (4–6). Standard therapies such as medication with exogenous mammalian surfactants are adequate to improve the condition of such disease patterns. However, none of these extracts achieve the efficiency of native human surfactant material (1). Thus the development of defined and efficient surfactant extracts is a major challenge within the investigations of therapeutic practices and requires a precise understanding of the function of the different lipid and protein constituents within the lung surfactant.

The main lipid component is phosphatidylcholine (PC), primarily the disaturated dipalmitoylphosphatidylcholine (DPPC). Pure DPPC is able to reduce the surface tension to near 0 mN/m and thus was often proposed to be the most important surface tension reducing component of lung surfactant (7–9). Nowadays the simple enrichment of DPPC during exhilaration with simultaneous squeeze out of other surfactant constituents is discussed critically; more complex mechanisms, such as the formation of coexistent DPPC-rich monolayer domains and three-dimensional lipid/protein regions, seem to be more likely (10). Other major lipid components are unsaturated, flexible PCs, which can provide the required fluidity during the dynamic breathing process, where the surface of the alveolar system decreases and increases alternately (11). The exact function of anionic phosphatidylglycerols (PGs), in particular the interaction with partly positively charged surfactant protein SP-B, is the focus of many recent investigations but is still considered controversial (12–14); despite this, these lipids contribute to general charge balancing in pulmonary surfactant.

Among the different lipid constituents, a protein content of ~10 wt % has been identified in mammalian surfactant systems (15,16). The hydrophilic proteins SP-A and SP-D, mainly located in the aqueous hypophase, are required for the immune response of the lung and for the storage and transport of surfactant material to the alveolar surface (17–19). The hydrophobic surfactant proteins SP-B and SP-C, mainly located in the surface film, are crucial elements for the absorption of surfactant material from the hypophase by inhalation as well as for the formation of surface-associated surfactant reservoirs by controlled squeeze out of, e.g., phospholipids during exhalation (3,7,20–23). Different studies show that a deficiency of SP-B and SP-C causes lethal respiratory distress syndrome, thus emphasizing the essential role of these peptides by maintaining the complete and well-structured coverage of the alveolar surface during the breathing process (6,24). Both proteins combine highly hydrophobic with hydrophilic regions, including even charged parts within their structure. This amphiphilic character predestines the

Submitted February 14, 2007, and accepted for publication April 11, 2007.

Address reprint requests to H.-J. Galla, Institute of Biochemistry, 48149 Münster, Germany. Tel.: 0049-251-833200; Fax: 0049-251-8333206; E-mail: gallah@uni-muenster.de.

Editor: Peter Hinterdorfer.

0006-3495/07/08/1192/12 $2.00

doi: 10.1529/biophysj.107.106765

peptides to array at membrane interfaces, e.g., the alveolar surface, by embedding the hydrophobic parts into the acyl chain regions, whereas the hydrophilic array is directed to the aqueous media (2).

The focus of this study is the surfactant protein SP-B, which is a homodimeric protein consisting of two small polypeptides of 79 amino acids with a molecular mass of 8.7 kDa. Containing seven cysteines, three intramolecular disulfide bridges stabilize the tertiary structure of the monomer, and one intermolecular bond forms the functional dimer (2, 21,25). Circular dichroism spectroscopy revealed a mainly α-helical structure (44%) with a contribution of 22% β-sheet secondary structure. The protein contains 4–5 amphipathic helices that allow interactions with lipid membranes. Besides a fraction of 52% hydrophobic amino acid residues, the peptide exhibits 6–7 positive net charges at physiological pH conditions within its structure (2,26,27). SP-B contributes to the stabilization of lung surfactant by formation of surface-associated surfactant reservoirs during exhalation. Scanning force microscopy (SFM) studies indicated these reservoirs to be lipid double layer structures below the surface film that are probably enriched in SP-B. These squeezed out lipid storages are reversibly rebuilt into the surface film by inhalation and increasing the alveolar surface, respectively (21).

Pivotal for the described SP-B function seem to be specific lipid/protein interactions. Regarding the two important lipid constituents DPPC and DPPG at moderate pH conditions, either the neutral DPPC (12) or the basically negatively charged DPPG (13) are proposed to be mainly colocalized or to interact preferentially with the partly positively charged peptide.

One elegant and reliable method to visualize the lateral organization and localization of surfactant components in a monolayer for gaining indications about specific interactions in the regarded system is the laterally resolved time-of-flight secondary ion mass spectrometry (TOF-SIMS) (12). By application of this potent technique, Breitenstein et al. (12) recently showed that SP-B does not colocalize with the negatively charged lipid DPPG in a DPPC/DPPG mixture when an aqueous subphase (pH 5.5) was used. These results seem to be contradictory to the ones presented by Pérez-Gil et al. (13) where an electrostatic DPPG/SP-B interaction was deduced indirectly from electron spin resonance experiments performed in a buffered system (pH 7.0). Since these investigations were accomplished with different experimental techniques at different measuring conditions (pH, membrane preparation, protein concentration), we decided to perform a systematic study of a model system consisting of surfactant components in native ratios (DPPC/DPPG/SP-B (4:1:0.2 mol %) (28)) at pH 5.5 and 7.0. Furthermore the properties of the pure lipid systems and a lipid mixture of DPPC and DPPG were scrutinized to allow a detailed and comparative interpretation of the pH influence.

Our results obtained from film balance measurements, fluorescence microscopy, SFM, and TOF-SIMS give strong indications that, at least in the chosen model system, no exclusive interaction of either DPPG or DPPC with SP-B exists. Rather, the phase behavior of the lipid components determines the localization of the protein in the lipid mixture, leading to a model, which describes the lipid/protein colocalization of SP-B in its surfactant environment.

MATERIAL AND METHODS

Materials

DPPC, DPPG (1,2-dipalmitoyl-*sn*-glycero-3-[phospho-*rac*-(1-glycerole)]) and palmitoyl chain-deuterated d62-DPPG were purchased from Avanti Polar Lipids (Alabaster, AL). Fluorophore-labeled lipid BODIPY-PC (2-(4,4-difluoro-5-methyl-4-bora-3a,4a-diaza-s-indacene-3-dodecanoyl)-1-hexadecanoyl-*sn*-glycero 3-phosphocholine) were obtained from Molecular Probes (Eugene, OR). All lipids were used without further purification.

SP-B was isolated from porcine bronchoalveolar lavage fluid by the butanol extraction method (29,30). Analysis of purity and sequence of the homodimer peptide is described elsewhere (12).

Organic solvents in high-performance liquid chromatography grade (chloroform, methanol, *n*-hexane), sodium hydroxide (per analysis) and hydrochloric acid (p.a.) were purchased from Merck (Darmstadt, Germany). Water was purified and deionized by a Millipore multi-cartridge system (Billerica, MA). HEPES (*N*-(2-hydroxyethyl)piperazine-*N*′-2-ethansulfonic acid) was obtained from Sigma-Aldrich (Taufkirchen, Germany).

Mica slides were purchased from Provac (Balzers/St. Gallen, Switzerland), and Tempax glass slides obtained from Rettberg (Goettingen, Germany). Chromium was received from Bal Tec (Balzers, FL), and gold was supplied by Degussa (Hanau, Germany).

Film balance measurements

All measurements were performed on a Wilhelmy film balance (Riegler and Kirstein, Mainz, Germany) with a Teflon trough area of 144 cm^2 at a temperature of 20°C. Pure lipid solutions of DPPC and DPPG, a lipid mixture of DPPC/DPPG in a molar ratio of 4:1, and a lipid/protein mixture of DPPC/DPPG/SP-B (4:1:0.2 mol % of the dimeric protein form) were prepared with chloroform/methanol (1:1, v/v) as solvent and spread on the film balance on 72 ml of either a pure water or a 0.1 mM HEPES buffer (pH 5.5/7.0) subphase. After 15 min of equilibration, the monolayers were compressed by the moveable barrier with a rate of 5.81 cm^2/min.

Fluorescence measurements

An amount of 0.5 mol % BODIPY-PC (solved in chloroform/methanol (1:1, v/v)) was added to solutions of DPPC, DPPG, a lipid mixture of DPPC/DPPG in a molar ratio of 4:1, and a lipid/protein composite of DPPC/DPPG/SP-B (4:1:0.2 mol % of the dimeric protein form) in chloroform/methanol (1:1, v/v). The fluorescence-dye-containing solutions were spread on a Wilhelmy film balance with a Teflon trough area of 144 cm^2 (Riegler and Kirstein, Mainz, Germany), equilibrated for 15 min, and compressed with a rate of 5.81 cm^2/min. In each case 72 ml of 0.1 mM HEPES buffer were used as subphase. At certain pressures the barrier was stopped and the surface films were visualized by application of fluorescence microscopy using a STM5-MJS fluorescence microscope (Olympus, Hamburg, Germany) and a charge-coupled device camera C4742-95 (Hamamatsu Photonics, Hersching, Germany).

Preparation of gold supports

Preparation of gold supports was accomplished by a method described by Bourdos et al. (31). Tempax glass slides were washed by sonification at 70°C in detergent and water alternately, every step three times. The slides were dried under nitrogen stream and then treated with argon plasma

(plasma cleaner, PDC 32G-2, Harrick, Ossening, NY) for 3 min. Afterward, a coating of 1 nm chromium (adhesive layer) was deposited onto the cleaned glass slides before a 200-nm-thick gold cover was sublimed onto the slides at a rate of 0.01 nm/s. The prepared gold supports were then cleaned for 8 h in a Soxhlet apparatus by using *n*-hexane as purification solvent, dried, and then directly employed for Langmuir-Blodgett (LB) transfers.

Langmuir-Blodgett transfers

As described by Ross et al. (32) LB transfers of a lipid/protein mixture DPPC/DPPG/SP-B (4:1:0.2 mol % of the dimeric protein form) dissolved in chloroform/methanol (1:1, v/v) onto either mica sheets (Provac) or gold supports were performed. The transfers were accomplished by using a Wilhelmy film balance (Riegler and Kirstein) with a Teflon trough area of 38.5 cm^2 and with 25 ml of a 0.1 mM HEPES subphase (pH 5.5/7.0) at a temperature of 20°C. The mica/gold substrates were dipped vertically into the subphase before spreading the sample solution. After an equilibration time of 15 min, the films were compressed with a rate of 1.5 cm^2/min until a surface pressure of $\gamma = 50$ mN/m was reached. Then the films were equilibrated for another 30 min and transferred onto the solid support with a lift velocity of 7×10^{-4} mm/min. For analyzing the quality of the transfers, the ratio of the area of immersed solid substrate and the area of transferred material was calculated. Only samples with a transfer rate >0.9 were used for further investigations.

Scanning force microscopy

Surface images of DPPC/DPPG/SP-B (4:1:0.2 mol % of the dimeric form) LB films on mica sheets were obtained by using a Nanoscope IIIa Dimension 300 microscope (Digital Instruments, Santa Barbara, CA). During all measurements the ratio of set amplitude A_{sp} to amplitude of vibration r was set to 0.4–0.7 (moderate tapping mode). The silicon cantilevers with a nominal spring constant of 40 (25–75) N/m and a resonance frequency of 300 ± 100 kHz were purchased from Budget Sensors (Sofia, Bulgaria).

Time-of-flight secondary ion mass spectrometry

All TOF-SIMS measurements of DPPC/d62-DPPG/SP-B (4:1:0.2 mol % of the dimeric protein form) LB films on gold supports were obtained with a TOF-SIMS IV (IONTOF, Münster, Germany) using Bi_3^+ as primary ion at 25 keV. Spectra were taken in bunched mode (focus: 3–5 μm) with a mass resolution of 5000–10,000. Cycling time of the instrument was set to 200 μs, allowing the acquisition of spectra up to a mass/charge ratio of 1800. Mass-resolved images were taken at nominal mass resolution (burst alignment mode, focus 300 nm). A surface of $(80)^2$ μm^2 was rastered with 128 × 128 pixels (pixel size: 625 nm). The primary ion dose did not exceed 8×10^{12} ions/cm^2. In line with observations of Biesinger et al. (33), at this primary ion dose no change or inversion of contrast could be detected in any of the measurements performed.

RESULTS

Surface pressure area isotherms

Application of film balance to amphiphilic systems offers a good facility to analyze the phase behavior of monolayers at the air/water interface depending on the available area. For our investigation of the pH influence on specific lipid/SP-B interactions, the native lung surfactant composite was reduced to a DPPC/DPPG/SP-B composition in naturally found ratios with a lipid molar ratio of 4:1 and a protein content of 0.2 mol % with respect to the lipid (28). Additionally, the pH influence on the phase behavior of pure lipid systems as well as of DPPC/DPPG (4:1) mixtures was analyzed by film balance measurements to provide comparability and a systematic investigation. Foremost, an adequate subphase buffer system had to be found which features a stable pH and comparability to the unbuffered watery subphase system used by Breitenstein et al. (12).

As shown in Fig. 1 *A*, 0.1 mM HEPES buffer has a slight influence on the phase behavior of a DPPC monolayer compared to an unbuffered water subphase. Despite the low HEPES concentration, the pH could be held constant for at least 1 h, which was convenient for carrying out the experiments. The DPPC isotherms on 0.1 mM HEPES exhibit rather small shifts of 2 $Å^2$ to higher molecular areas over the whole pressure range. The surface pressure of the plateau in the liquid-expanded/liquid-condensed (LE/LC) main phase transition region is slightly increased by 2 mN/m to ~8 mN/m, whereas the plateau of the buffered systems shows a slope that is a little higher (less compressibility) than the DPPC isotherm on a pure water subphase. The difference due to the pH change is even less pronounced; however, a slight fluidization effect due to the HEPES molecules at pH 5.5 compared to the pH 7.0 system can be recognized in an increase of the mean plateau surface pressure by 1 mN/m.

Fig. 1 *B* shows a distinct pH influence on the phase behavior of DPPG monolayers. An increase of pH is followed by expansion and fluidization of the films over the whole measuring range. Higher pH values lead to a shift of the isotherms to higher molecular areas. While at pH 4.0 no typical LE/LC phase transition plateau appears, at higher pH values the main phase LE/LC transition can be observed at surface pressures of 2.5 mN/m (pH 5.5), 3.5 mN/m (pH 7.0), 6.5 mN/m, and 10.5 mN/m (pH 8.0), respectively.

Regarding the DPPC/DPPG 4:1 mixture (Fig. 1 *C*), again expansion and fluidization of the surface film due to a pH increase can be determined. Comparable to the pure DPPG system, the pH 7.0 isotherm exhibits a higher surface pressure (~1 mN/m) in the plateau region and a small shift to higher molecular areas (~1–2 $Å^2$), even though the effect is less pronounced in the 4:1 mixture.

In the complete model system of DPPC/DPPG/SP-B (4:1:0.2 mol % of the dimeric protein form), again a fluidization tendency at pH 7.0 compared to pH 5.5 can be found (Fig. 1 *D*). Although the isotherm at pH 7.0 shows a distinct low pressure plateau at a surface pressure of ~7 mN/m, no such clear indication for a lipid LE/LC phase transition can be observed at pH 5.5. Additionally, the kink at a surface pressure of ~40 mN/m, which is generally attributed to a material squeeze out induced by SP-B (21), is slightly more pronounced at pH 7.0.

Fluorescence images

Fluorescence microscopy was applied to visualize the phase behavior of the lipid systems and the DPPC/DPPG/SP-B (4:1:0.2 mol % of the dimeric protein form) model system,

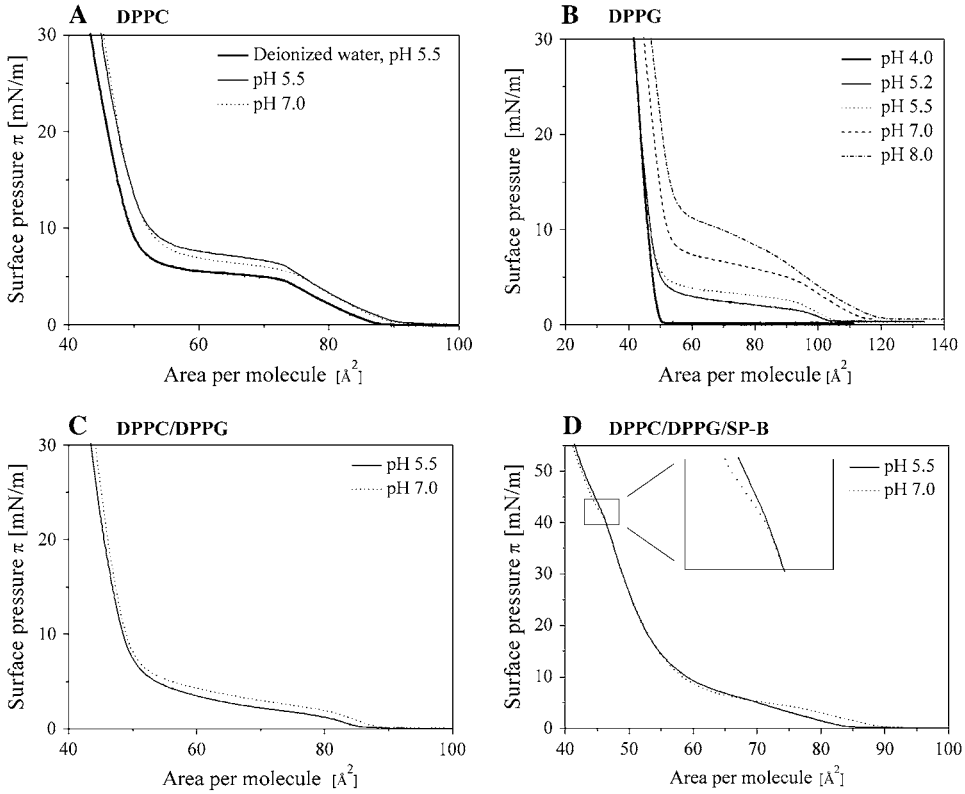

FIGURE 1 Compression π-A isotherms of different lipid and lipid/SP-B monolayer systems at different pH and a temperature of 20°C. If not indicated otherwise, all measurements were accomplished on 0.1 mM HEPES buffer as subphase. (*A*) DPPC, (*B*) DPPG, (*C*) DPPC/DPPG in a molar ratio of 4:1, and (*D*) DPPC/DPPG/SP-B (4:1:0.2 mol % of the dimeric protein form).

respectively. The analysis of the LE/LC phase transition of amphiphilic systems can be accomplished by screening the distribution of the fluorescence dye in the lipid film. The contrast of fluorescence images depends on the different solubility of the dye in the LE and LC phase of the monolayer system. The LE phase is observed as homogeneous, bright surface regions due to rather loosely lipid packing and a more disordered orientation of the acyl chains, thus leading to an inclusion and penetration of the dye into this phase. By compressing the surface film, characteristically shaped LC domain areas can be found as dark spots in the bright LE bulk, which grow due to further compression and increase of surface pressure, respectively. The dye cannot penetrate in this tightly packed phase where the acyl chains are ordered in a definite pattern and strong intermolecular forces exist. In high compressed states of the surface film, the whole system exists in condensed or even solid analog phase. Under these film conditions the direct vicinity (distance within the Förster radius) and clearly structured orientation of the dye molecules to each other leads to self-quenching processes of the dye and thus to a rapidly decreasing contrast of fluorescence images (22,34).

Fig. 2 shows fluorescence images of pure DPPC and DPPG monolayers as well as from the lipid mixture DPPC/DPPG in a molar ratio of 4:1. In the DPPC monolayer, liquid condensed regions are not formed until reaching a surface pressure of 6 mN/m at both pH conditions (Fig. 2 *A*). By compressing the system, the formed LC-domains grow up to a diameter of 20–25 μm, whereas the number of domains stays rather constant. The domains can be described as kidney- and wavelike-shaped structures arranged in two- or threefold rotation-symmetric assemblies of counterclockwise direction representing the chirality of the DPPC molecules. Pictures at a surface pressure of 20 mN/m show the described contrast leakage due to a condensed state of the whole film and self-quenching processes of the dye, respectively.

In contrast the DPPG constitutes condensed lipid domains even under highly expanded film conditions (Fig. 2 *B*). Compared to the DPPC monolayers, the domain size ($<$5 μm) is much smaller, whereas the number of LC phases is considerably increased. Within the DPPG images, a clear tendency to fluidization and expansion of the surface films due to an increase of the pH can be observed. At a particular surface pressure, a pH rise leads to a considerably decreased domain size, whereas the fraction of bright LE phase is increased. For example at pH 4.0, the whole system is already condensed at a surface pressure of 5 mN/m (contrast leakage, high dark image fraction), whereas at pH 8.0 this state is hardly reached at surface pressures of $\sim$10–20 mN/m.

In the 4:1 mixture of DPPC and DPPG, a clear pH effect can be identified as well (Fig. 2 *C*). At pH 5.5 circular LC domains are formed, whereas at pH 7.0 kidney- and wavelike-shaped structures are established. On the contrary, number and size ($\sim$10–15 μm in diameter at a surface pressure of 10 or 20 mN/m) of LC domains stay rather constant and are intermediate in the number and size of DPPC and DPPG domains.

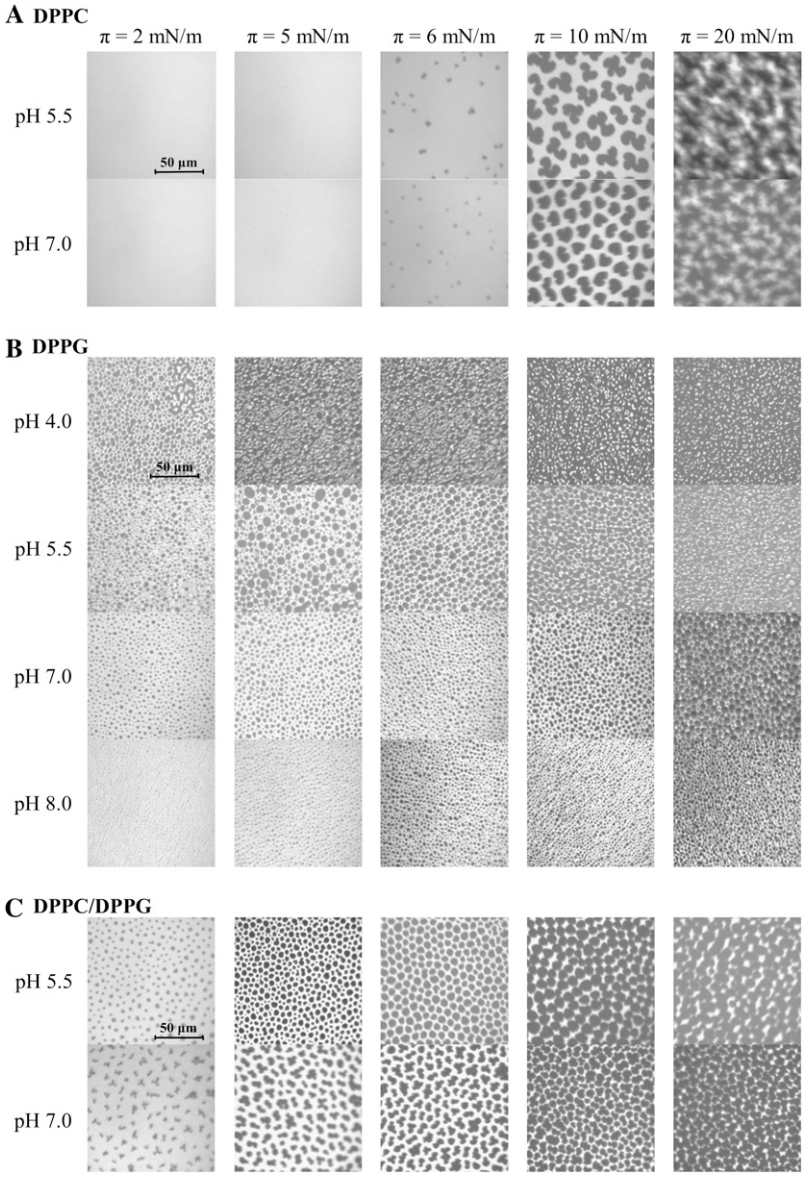

FIGURE 2 Fluorescence images of different lipid monolayer systems at different pH on 0.1 mM HEPES buffer as subphase at a temperature of 20°C. Pictures at different surface pressures are shown. All samples contained a fraction of 0.5 mol % fluorescence dye BODIPY-PC. (*A*) DPPC, (*B*) DPPG, and (*C*) DPPC/DPPG in a molar ratio of 4:1.

Scanning force microscopy

The SFM technique allows us to see the topography, friction, or viscoelasticity parameters of any solid supported system in high lateral resolution. In our case, we used SFM to clarify the topographic properties of DPPC/DPPG/SP-B (4:1:0.2 mol % of the dimeric protein form) systems under high pressure depending on a pH variation. Figs. 3 and 4 show SFM images of such surface films transferred to mica at a surface pressure of 50 mN/m from 0.1 mM HEPES buffer either at pH 5.5 (Fig. 3) or 7.0 (Fig. 4) at a temperature of 20°C in different lateral resolutions. The surface films show both similarities and differences in the topography due to a pH change. At either pH condition, in particular the 20 × 20 μm^2 images show a uniform pattern of three-dimensional structures. The pictures reveal domains with a diameter of 1–3 μm, which are surrounded by a consistent network of ~5 nm higher structures. These structural facts can be correlated to fluorescence images of compressed DPPC/DPPG/SP-B (4:1:0.2 mol % of the dimeric protein form) surface films on 0.1 mM HEPES buffer at a surface pressure of 50 mN/m and a temperature of 20°C (Fig. 5). Although the diameters of dark domains correspond to the lower height regions of the SFM images, the bright film areas, which obviously contain the fluorescence dye, match with the elevated network structure. At a surface pressure of 50 mN/m the whole film is present in a condensed state; however, the dye-containing network marks these film regions as the last condensed areas. A more accurate analysis of the described protrusions is provided by the higher resolved SFM images (Figs. 3, *B* and *C*, and 4, *B* and *C*) with scales of 5 × 5 μm^2

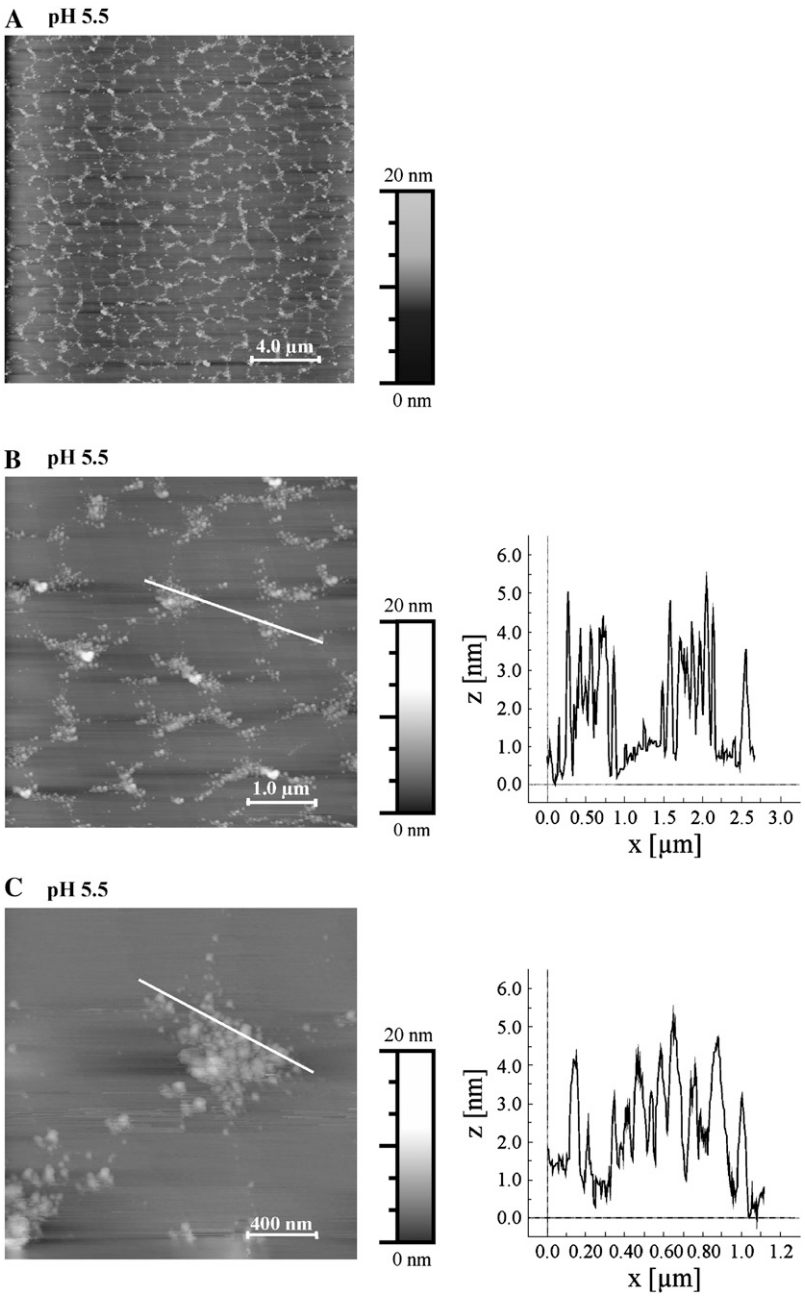

FIGURE 3 SFM images of a DPPC/DPPG/SP-B (4:1:0.2 mol % of the dimeric protein form) monolayer. The surface film was transferred by LB transfer at a temperature of 20°C and a surface pressure of 50 mN/m from 0.1 mM HEPES buffer/pH 5.5 to a mica slide. The image sizes are $20 \times 20\ \mu m^2$ (*A*), $10 \times 10\ \mu m^2$ (*B*), and $5 \times 5\ \mu m^2$ (*C*). *B* and *C* also show the height profile along the drawn contour line.

and $2 \times 2\ \mu m^2$, respectively. The network consists of rather circular, colocalized structures with a height of 4–5 nm, which corresponds to the thickness of a lipid double layer. SP-B containing lipid films are different with respect to the size of these protrusions. Although at pH 5.5 diameters of ~50–70 nm were observed, the images of transferred surface films at pH 7.0 show an enlargement to ~120–150 nm.

Time-of-flight secondary ion mass spectrometry

By application of laterally resolved TOF-SIMS, the imaging of variable probes on a molecular level is possible. We used this technique to analyze the molecular distribution of the different constituents in the surfactant model system DPPC/d62-DPPG/SP-B (4:1:0.2 mol % of the dimeric protein form). Since DPPG does not yield any specific positive headgroup fragment ions, palmitoyl chain deuterated d62-DPPG was used for clear distinction between the two lipid components (31). This is an appropriate substitution, since it is known that the phase behavior properties of deuterated d62-DPPG do not deviate from properties of DPPG (12). Fig. 6 shows the mass spectrum of positive fragment ions from a DPPC/d62-DPPG/SP-B probe with classification of some mass peaks by the empirical formula. As can be seen from the spectrum, the signals show distinctly different intensities due to fragmentation and ionization affinity. In Fig. 7

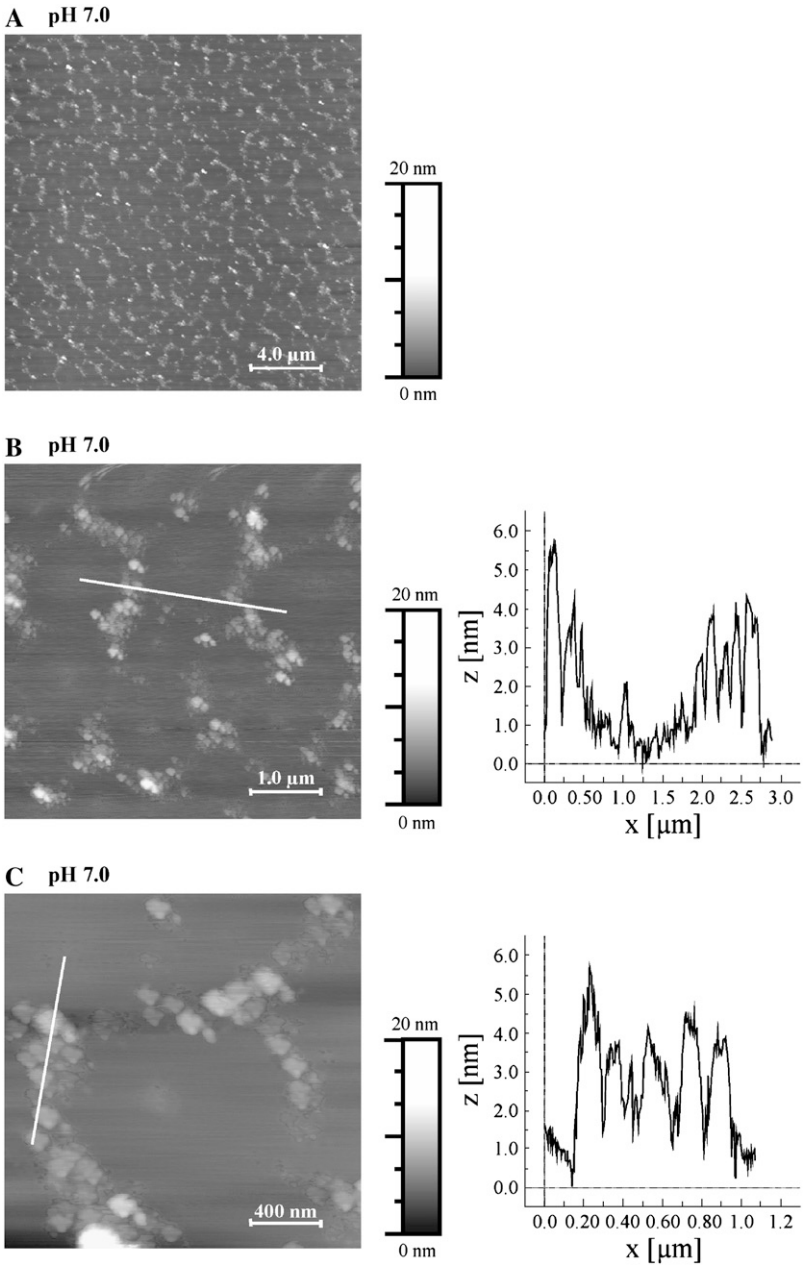

FIGURE 4 SFM images of a DPPC/DPPG/SP-B (4:1:0.2 mol % of the dimeric protein form) monolayer. The surface film was transferred by LB transfer at a temperature of 20°C and a surface pressure of 50 mN/m from 0.1 mM HEPES buffer/pH 7.0 to a mica slide. The image sizes are $20 \times 20\ \mu m^2$ (*A*), $10 \times 10\ \mu m^2$ (*B*), and $5 \times 5\ \mu m^2$ (*C*). *B* and *C* also show the height profile along the drawn contour line.

specific *m/z* ratios and mass peaks with rather high signal intensities, respectively, are attributed to a particular film component. DPPC can be specified by two fragment ions from its choline headgroup ($m/z(C_5H_{13}PNO_3^+) = 166$, $m/z(C_5H_{15}PNO_4^+) = 184$), whereas the d62-DPPG distribution images are due to its fragment ions of the deuterated fatty acyl chain ($m/z(C_2D_5^+) = 34$, $m/z(C_3D_7^+) = 46$). The SP-B distribution can be identified by specific fragment ions of amino acids (e.g., m/z $(C_4H_8N^+) = 70$ as fragment of proline).

At both pH conditions (pH 5.5 and 7.0), separated d62-DPPG domains with a diameter of $<5\ \mu m$ can be observed, indicated by the bright yellow color and a high counting rate of the specific ions, respectively. In comparison, the DPPC-specific signals demonstrate an inverse color and counting rate distribution, indicating a phase separation of the two lipid components in the chosen model system. Except for the d62-DPPG-rich domains, the bulk of the surface film shows a relatively high DPPC-specific fragment ion counting rate. The specific fragment ions of SP-B show a slightly diffuse distribution due to the low fraction of peptide in the sample; however, a detailed image comparison identifies an overlay of DPPC- and SP-B-specific secondary ion-rich film regions. Fig. 8 displays the fragment ion distribution in a varied way. Besides a display of one specific secondary ion distribution for each film component in a definite background color, an

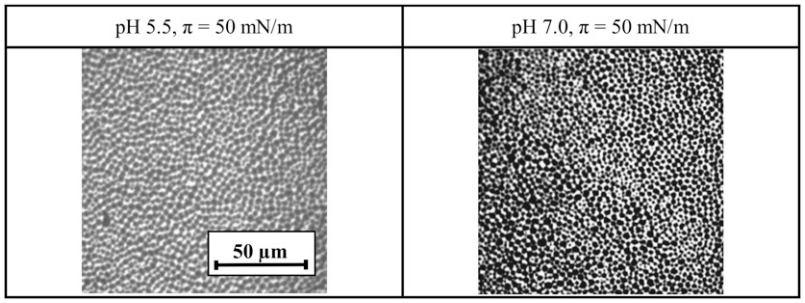

FIGURE 5 Fluorescence images of DPPC/DPPG/SP-B (4:1:0.2 mol % of the dimeric protein form) monolayers at different pH on 0.1 mM HEPES buffer as subphase at a surface pressure of 50 mN/m and a temperature of 20°C. Pictures at different surface pressures are shown. All samples contained a fraction of 0.5 mol % fluorescence dye BODIPY-PC.

overlay of these three images is presented to accurately show the distribution of all film constituents with respect to each other (correlation analysis). Here, the overlay clearly exhibits separated d62-DPPG domains with a diameter of <5 μm (*green color*) in a DPPC/SP-B bulk of the surface film (*pink colored regions* as an *overlay* of *red* and *blue*).

DISCUSSION

In this study, we analyzed a surfactant model system consisting of the two important lipid components DPPC and DPPG as well as of the surfactant protein SP-B. The focus of the investigation was the clarification of specific lipid/protein interactions and colocalizations, respectively. By using low concentrated HEPES buffer (0.1 mM) as the film balance subphase, a stable pH could be ensured for all measurements. Additionally, comparability to an unbuffered water subphase was provided by the used buffer system, even if a slight expansion and fluidization effect due to a HEPES adsorption at the lipid interface can be determined from DPPC isotherms (Fig. 1 *A*).

In the following discussion about pH influences, we will argue against the apparent pK_a, which is the measured or calculated pK_a with respect to the pH of the bulk solution. In

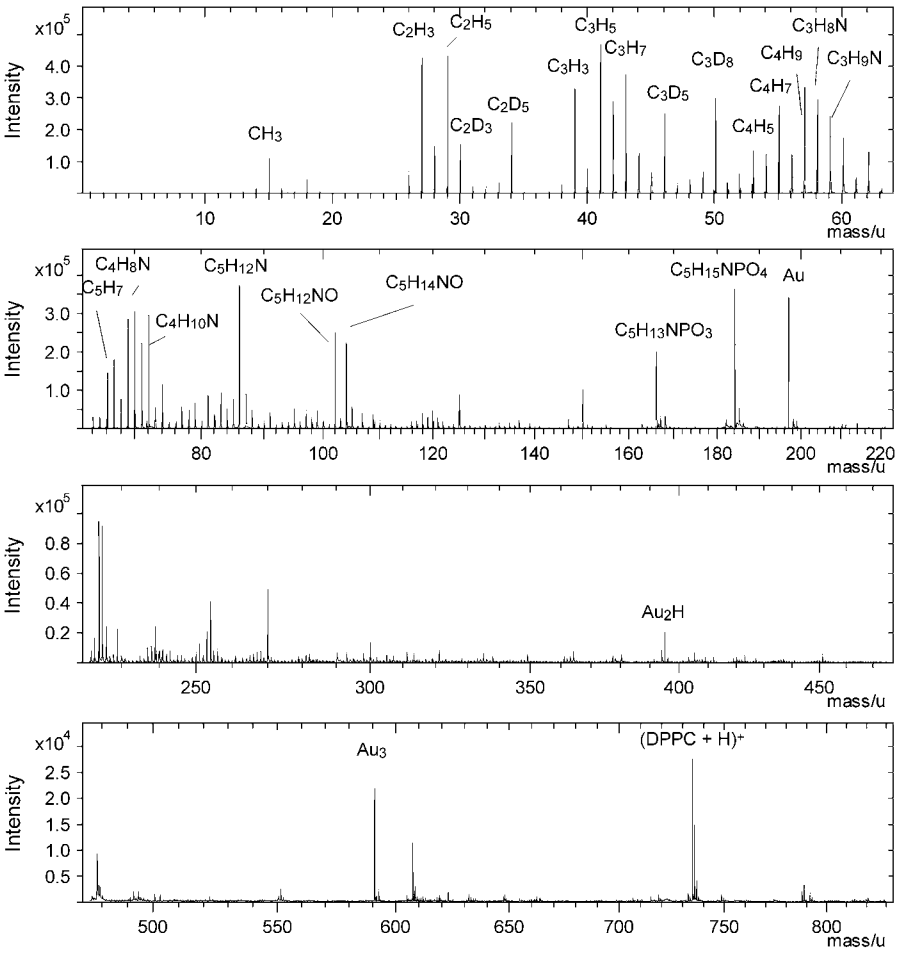

FIGURE 6 TOF-SIMS spectrum of singly positively charged secondary ions of a DPPC/d62-DPPG/SP-B (4:1:0.2 mol % of the dimeric protein form) probe on gold support. The mass peaks correspond to the components of the surface film. Each mass peak and *m*/*z* ratio, respectively, can be attributed to a specific film component. For correlation, see Figs. 7 and 8.

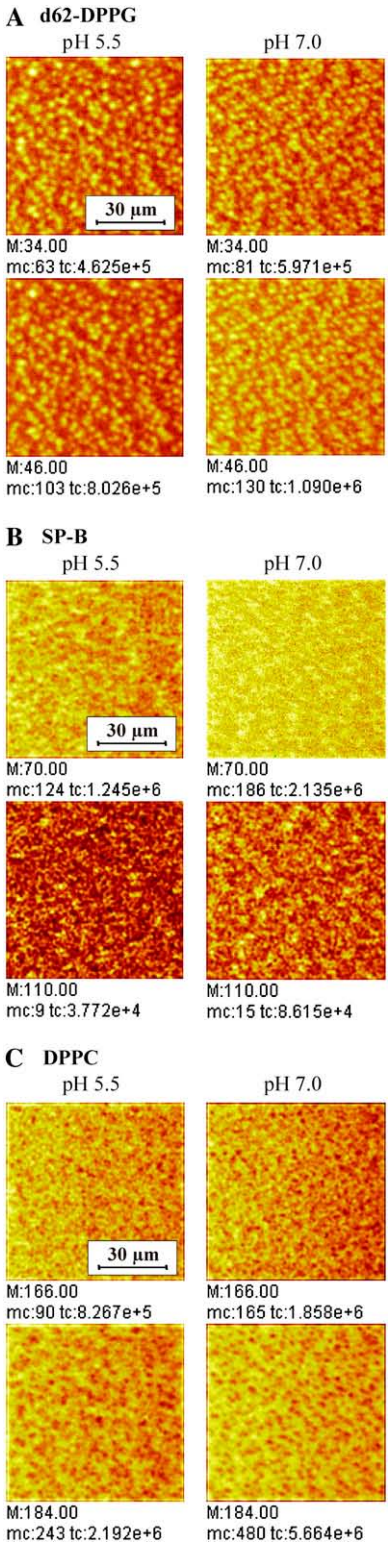

FIGURE 7 Depiction of DPPC/d62-DPPG/SP-B (4:1:0.2 mol % of the dimeric protein form) surface films by TOF-SIMS in lateral resolution after LB transfer from 0.1 mM HEPES buffer (pH 5.5 and pH 7.0) at a surface pressure of 50 mN/m and a temperature of 20°C. The distribution of two fragment secondary ions (specified by the mass/charge ratio (*m/z*)) of each film component is shown: *m/z* of 34 ($C_2D_5^+$) and 46 ($C_3D_7^+$) are d62DPPG specific; *m/z* of 70 ($C_4H_8N^+$) and 110 ($C_5H_8N_3^+/C_7H_{12}N^+$) are SP-B specific; *m/z* of 166 ($C_5H_{13}PNO_3^+$) and 184 ($C_5H_{15}PNO_4^+$) are DPPC specific. Light colored film regions correspond to a high counting rate of a particular fragment ion, whereas darker areas are due to a lower counting rate.

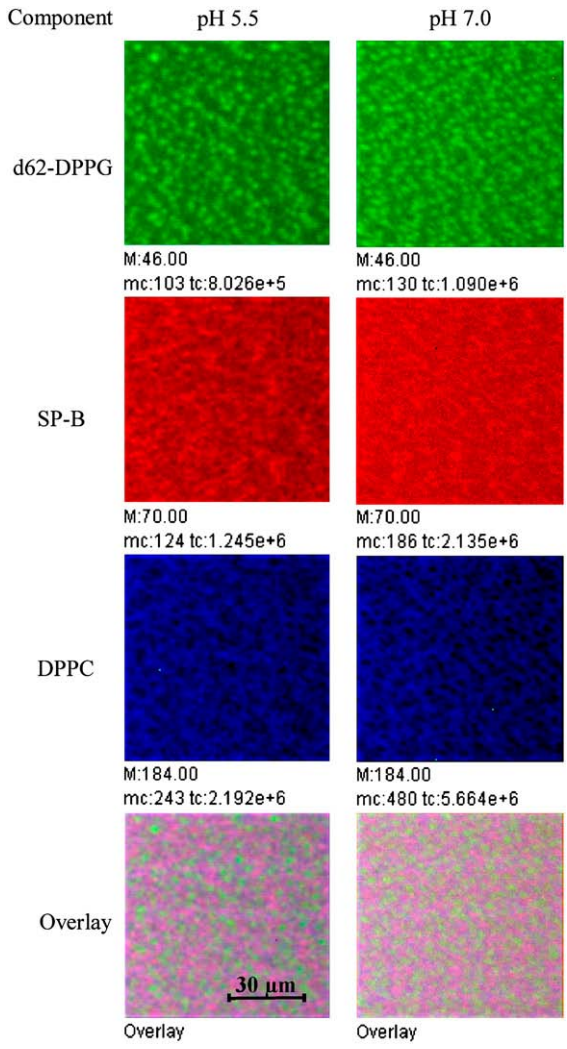

FIGURE 8 Varied depiction of fragment secondary ion distribution of DPPC/d62DPPG/SP-B (4:1:0.2 mol % of dimeric protein form) surface films. For each film component, one specific fragment ion distribution in distinguishable main color is shown (compare Fig. 7). Additionally, an image overlay is displayed.

contrast, the intrinsic pK_a, which is the pK_a with respect to the pH at the regarded lipid interface, considers interface effects such as surface potentials, intermolecular interactions like hydrogen bonds, or electrostatic forces and dielectricity. The accurate calculation of these interface properties is rather delicate and underlies mathematical approximations. A convenient explanation of all these effects can be found elsewhere (35–37).

Since the pK_a of PC or the complete lipid DPPC in a monolayer was calculated to be ~1–3 (35), no change in the protonation state of the lipid can be expected by varying the pH between 5.5 and 7.0. In contrast a full deprotonation and thus only dipolar DPPC molecules with no net charge have to be assumed at either pH condition. The difference between the DPPC isotherms due to a pH change can be explained by the protonation state of the buffer molecule HEPES with a pK_a of 7.55. Although the dipolar ion exists almost exclusively at pH 5.5, at pH 7.0 the dipolar fraction is clearly decreased (ratio of dipolar ion/anion is 3:1, application of the Henderson-Hasselbalch equation). The dipolar HEPES ion can much better incorporate and penetrate electrostatically into the lipid monolayer consisting also of dipolar DPPC molecules, which leads to the more pronounced fluidization effect at pH 5.5.

The distinct expansion and fluidization of DPPG monolayers due to a pH increase can be determined from Fig. 1 *B*. The negative charge of DPPG in the deprotonated state causes a negative surface potential, which leads to an enrichment of positive charges, e.g., protons, at the monolayer interface (35–37). This proton gradient is responsible for a low deprotonation grade and a high pK_a of DPPG, respectively. The Boltzmann equation describes the proton distribution between interface and bulk solution quantitatively (35,37):

$$pH_{interface} - pH_{bulk} = \frac{e\psi_0}{2.3\,kT},$$

with e = elementary charge [C], ψ_0 = surface potential [V], $k \equiv$ Boltzmann constant $= 1.38 \times 10^{-23}$ J/K, and T = temperature [K].

The pK_a of DPPG in a monolayer is calculated to be ~4–5 (36). Thus a pH variation from pH 4.0–8.0 leads to a clear difference in the protonation state of DPPG and negative charge density in the monolayer, respectively. The more negatively charged lipid molecules in the monolayer there are, the more electrostatic repulsion between the molecules must be expected. The direct consequence is the fluidization effect shown in Fig. 1 *B*.

Even in DPPC/DPPG (4:1) mixtures the influence of the DPPG protonation state can be observed in the isotherms (Fig. 1 *C*), even though the expansion is less pronounced due to the low fraction of only 20 mol % DPPG in the monolayers.

The isotherms of the complete model system DPPC/DPPG/SP-B also show a pH influence in the lipid phase transition region. Comparable to the pure DPPG system and the DPPC/DPPG mixture, at pH 7.0 a clear LE/LC phase transition plateau can be observed. In contrast, at pH 5.5 the less pronounced phase transition plateau of the lipids cannot be seen in the isotherm of the peptide-containing model system. This result indicates the phase properties of DPPG in the isotherm and might be a hint for a phase separation of DPPG in the model system; however, this effect is only assumed and not proven yet.

The fluorescence images of the lipid systems and mixture shown in Fig. 2 are convenient to verify the mentioned lipid phase separation. In the DPPC monolayer, condensed regions are not formed until reaching a surface pressure of 6 mN/m at both pH conditions. In more expanded states the surface films are constituted in a homogeneous LE phase, indicated by the uniform distribution of the fluorescence dye and a complete brightness of the images (Fig. 2 *A*).

In contrast to DPPC, DPPG spontaneously constitutes condensed lipid domains even under highly expanded film conditions (Fig. 2 *B*). This result can be explained by a complex hydrogen-bond network in DPPG monolayers induced by the glycerol-containing headgroups evidenced by infrared spectroscopy (38,39). Besides the formation of such LC domains in the low surface pressure range, the spontaneous condensation leads to the rather high number of LC regions. Consequently, within these microscopic domains the pressure conditions differ from the macroscopic bulk system. In agreement with the film balance measurements, the fluorescence images confirm the fluidization effect due to a pH increase. At the same surface pressure conditions, the systems with higher pH show a considerably smaller fraction of condensed film regions. Additionally, the LC domain size is clearly decreased (Fig. 2 *B*). The higher charge density in the surface film at higher pH due to a correspondingly increased deprotonation state of DPPG leads to more electrostatic repulsion and higher surface potential energy in the system, especially in the rigid and tight LC regions. Thus the system corresponds by forming smaller LC domains.

The shown data of pure lipid systems indicate that DPPG mainly forms the centers of the condensed domains observed in the 4:1 lipid mixture, whereas DPPC probably accumulates to already existing domains at higher surface pressures and thus establishes the outer spheres. The shape difference of the condensed DPPC/DPPG structures at different pH values supports this assumption (Fig. 2 *C*). Two antagonistic effects have to be considered by regarding the shape profile of condensed domains in surface films. On the one hand, the line tension (comparable to the surface tension in three-dimensional) is responsible for the lowest borderline/area ratio of LC domains, thus leading to circular structures. On the other hand, electrostatic repulsion and dipole density in condensed surface film regions lead to more relaxed structured domains with a higher borderline/area ratio to avoid minimal distance between molecules (40,41). Although at pH 5.5 circular LC domains are formed (induced by the line tension), the electrostatic repulsion between the higher fraction of deprotonated DPPG molecules at pH 7.0, located in the centers of LC domains, leads to more relaxed, noncircular-shaped LC structures. The presented data show a clear instance for the two antagonistic effects of line tension and electrostatic repulsion and finally denote a phase separation of DPPC and DPPG in lipid monolayers.

Furthermore, SFM studies were performed to reveal the topographic conditions of SP-B-containing DPPC/DPPG

(4:1) monolayer systems. At both pH conditions the presented SFM images show a uniform network of colocalized, circular structures with a height of 4–5 nm, which is equivalent to the thickness of a lipid double layer (Figs. 3 and 4). This result supports the known SP-B function to form lipid reservoirs under the surfactant film (21). The clear difference lies in the diameter of these protrusions due to the chosen pH conditions: Broader structures at pH 7.0 refer to a higher amount of lipids in these protrusions than at pH 5.5. This finding is supported by the shown isotherms of the complete model system (Fig. 1 *D*), where a more distinct kink at a surface pressure of ~40 mN/m can be observed at pH 7.0 compared to pH 5.5. Thus at pH 7.0 more lipid molecules are squeezed out from the monolayer than at pH 5.5. Considering the spontaneous formation of condensed film regions of DPPG even under expanded film conditions (Fig. 2 *A*) due to a hydrogen-bond network (38,39), the protrusions probably refer mainly to DPPC as a squeezed-out lipid component in the chosen model system.

Additionally, the whole structure of the DPPC/DPPG/SP-B surface film can be understood by comparison of SFM (Figs. 3 and 4) and fluorescence images (Fig. 5). The diameters of the low film regions in the SFM correlate with the dark domains in the fluorescence images, whereas the higher areas of colocalized circular protrusions (SFM) match with the bright network (fluorescence microscopy). Former fluorescence studies evidenced the SP-B localization in surfactant model systems to be in the expanded film regions and the areas condensed last at high compression states, respectively (22,42). The observed correlation proves a clear distribution of the peptide SP-B in the surface films: First at either pH (pH 5.5 and 7.0) the protein is excluded from the condensed film regions; second it is incorporated into the less condensed areas and forms the mentioned protrusions in high compressed film states.

Laterally resolved TOF-SIMS allows the chemical analysis of the component distribution by detecting substance-specific fragment ions. The presented images clearly show separated areas with high counting rates of d62-DPPG-specific fragment ions in a DPPC/SP-B-rich bulk at both pH conditions (Figs. 7 and 8). It has to be mentioned that TOF-SIMS is not an absolutely quantitative technique. The matrix effect accounts for different fragmentation affinities of one kind of secondary ion in different chemical environments (12,43). In addition, the structural terms and conditions may play a role; e.g., the detection rate of fragment ions in multilayer structures is decreased by a factor of 1.5–5 compared to monolayer regions (44). This means that the low counting rate of d62-DPPG-specific signals outside the separated domains might be due to the formation of SP-B-containing double layer structures, which were evidenced by SFM. Nonetheless, a high fraction of d62-DPPG is definitely located in separated domains and thus not colocalized with the peptide SP-B. Since the phase behavior of DPPG and d62-DPPG were proven to be almost identical (12), the exchange with deuterated DPPG is reasonable for analyzing the molecular distribution in the intrinsic model system DPPC/DPPG/SP-B.

In summary, the TOF-SIMS clearly shows a phase separation of DPPC and d62-DPPG and provides final proof for the exclusion of SP-B from DPPG-rich domains of the pH. Moreover, an overlay of film regions with high counting rates of DPPC- and SP-B-specific fragment ions demonstrates a preferred colocalization of DPPC and SP-B in the chosen model system.

CONCLUSION

The existence of specific interactions between SP-B and negatively charged PGs has been controversial for some time. The influence of subphase pH on electrostatic interactions between these two surfactant components was especially an ambiguous reason for why we performed systematic studies with DPPC/DPPG/SP-B monolayers at two different pH values (5.5 and 7.0). Our results provide reliable proof for a considerable phase separation between DPPG and DPPC/SP-B, which is of the pH and most probably due to an extended hydrogen-bond network bridging the negatively charged lipid molecules. The solubility of SP-B in such dense DPPG domains is naturally low, which is the reason the protein is found in the surrounding DPPC bulk. Unlike the rigid, condensed DPPG-rich film regions, the more fluid lipid phase does not hinder but facilitates the flexibility of the protein to arrange in its optimal assembly at the air/water interface. The amphiphatic helices interact with the hydrophobic acyl chains of the lipids as well as with the hydrophilic headgroups and the aqueous subphase (2). By compression of the surface film and thus alteration of the DPPC/SP-B-rich phase into condensed film regions, the protein can react on these changing conditions, e.g., by lowering the hydrophilic parts into the subphase (U. Klenz, M. Saleem, M. C. Meyer, and H.-J. Galla, unpublished observation). This process leads to an ideal alignment of SP-B for interacting with the closely packed acyl chains of lipids and thus to the formation of above described protrusions as surfactant reservoirs. Our results, however, do not exclude the general existence of specific PG-SP-B interactions, especially in the case of unsaturated PGs. These more fluid lipids do not pack as tightly as DPPG and should provide a higher solubility of SP-B in PG-rich phases. Specific interactions—if they exist—should be detectable in such a model system.

REFERENCES

1. Alonso, C., T. Alig, J. Yoon, F. Bringezu, H. Warriner, and J. A. Zasadzinski. 2004. More than a monolayer: relating lung surfactant structure and mechanics to composition. *Biophys. J.* 87:4188–4202.
2. Serrano, A. G., and J. Pérez-Gil. 2006. Protein-lipid interactions and surface activity in the pulmonary surfactant system. *Chem. Phys. Lipids.* 141:105–118.

3. Galla, H.-J., N. Bourdos, A. von Nahmen, M. Amrein, and M. Sieber. 1998. The role of pulmonary surfactant protein C during the breathing cycle. *Thin Solid Films*. 327–329:632–635.
4. Avery, M. E., and J. Mead. 1959. Surface properties in relation to atelectasis and hyaline membrane disease. *AMA J. Dis. Child.* 97:517–523.
5. Jobe, A. H. 1993. Pulmonary surfactant therapy. *N. Engl. J. Med.* 328: 861–868.
6. Hallmann, M., V. Glumoff, and M. Ramet. 2001. Surfactant in respiratory distress syndrome and lung injury. *Comp. Biochem. Physiol. A Mol. Integr. Physiol.* 129:287–294.
7. Cruz, A., L. A. Worthman, A. G. Serrano, C. Casals, K. M. Keough, and J. Pérez-Gil. 2000. Microstructure and dynamic surface properties of surfactant protein B/dipalmitoylphosphatidylcholine interfacial films spread from lipid-protein bilayers. *Eur. Biophys. J.* 29:204–213.
8. Wustneck, R., J. Pérez-Gil, N. Wustneck, A. Cruz, V. B. Fainerman, and U. Pison. 2005. Interfacial properties of pulmonary surfactant layers. *Adv. Colloid Interface Sci.* 117:33–58.
9. Schürch, S., R. Qanbar, H. Bachofen, and F. Possmayer. 1995. The surface-associated surfactant reservoir in the alveolar lining. *Biol. Neonate*. 67:61–76.
10. Piknova, B., W. R. Schief, V. Vogel, B. M. Discher, and S. B. Hall. 2001. Discrepancy between phase behaviour of lung surfactant phospholipids and the classical model of surfactant function. *Biophys. J.* 81:2172–2180.
11. Takamato, D. Y., M. M. Lipp, A. von Nahmen, K. Y. C. Lee, A. J. Waring, and J. A. Zasadzinski. 2001. Interaction of lung surfactant proteins with anionic phospholipids. *Biophys. J.* 81:153–169.
12. Breitenstein, D., J. J. Batenburg, B. Hagenhoff, and H.-J. Galla. 2006. Lipid specificity of surfactant protein B studied by time-of-flight secondary ion mass spectrometry. *Biophys. J.* 91:1347–1356.
13. Pérez-Gil, J., C. Casals, and D. Marsh. 1995. Interactions of hydrophobic lung surfactant proteins SP-B and SP-C with dipalmitoylphosphatidylcholine and dipalmitoylphospatidylglycerol bilayers studied by electron spin resonance spectroscopy. *Biochemistry.* 34:3964–3971.
14. Pérez-Gil, J. 2001. Lipid-protein interactions of hydrophobic proteins SP-B and SP-C in lung surfactant assembly and dynamics. *Pediatr. Pathol. Mol. Med.* 20:445–469.
15. Batenburg, J. J. 1992. Surfactant phospholipids: synthesis and storage. *Am. J. Physiol.* 262:L367–L385.
16. King, R. J. 1982. Pulmonary surfactant. *J. Appl. Physiol.* 53:1–8.
17. Creuwels, L. A. J. M., L. M. G. van Golde, and H. P. Haagsman. 1997. The pulmonary surfactant system: biochemical and clinical aspects. *Lung*. 175:1–39.
18. Johansson, J., and T. Curstedt. 1997. Molecular structures and interactions of pulmonary surfactant components. *Eur. J. Biochem.* 244: 675–693.
19. Van Rozendaal, A. V., C. H. Van De Lest, M. Van Eijk, H. P. Van Helden, and H. P. Haagsman. 1997. Pulmonary surfactant proteins A and D are involved in the early response to intracheally aerosolized lipopolysaccharide. *Biochem. Soc. Trans.* 25:656–664.
20. Nag, K., G. Munro, K. Inchley, S. Schurch, N. O. Petersen, and F. Possmayer. 1999. SP-B refining of pulmonary surfactant phospholipid films. *Am. J. Physiol.* 277:L1179–L1189.
21. Krol, S., M. Ross, M. Sieber, S. Künneke, H.-J. Galla, and A. Janshoff. 2000. Formation of three-dimensional protein-lipid aggregates in monolayer films induced by surfactant protein B. *Biophys. J.* 79:904–918.
22. Von Nahmen, A., A. Post, H.-J. Galla, and M. Sieber. 1997. The phase behaviour of lipid monolayers containing pulmonary surfactant protein C studied by fluorescence light microscopy. *Eur. Biophys. J.* 26:359–369.
23. Von Nahmen, A., M. Schenk, M. Sieber, and M. Amrein. 1997. The structure of a model pulmonary surfactant as revealed by scanning force microscopy. *Biophys. J.* 72:463–469.
24. Klein, J. M., M. W. Thompson, J. M. Snyder, T. N. George, J. A. Whitsett, E. F. Bell, P. B. McCray Jr., and L. M. Nogee. 1998. Transient surfactant protein B deficiency in a term infant with severe respiratory failure. *J. Pediatr.* 132:244–248.
25. Vandenbussche, G., A. Clercx, M. Clercx, T. Curstedt, J. Johansson, H. Jörnwall, and J.-M. Ruysschaert. 1992. Secondary structure and orientation of the surfactant protein SP-B in a lipid environment. A Fourier transform infrared spectroscopy study. *Biochemistry*. 31:9169–9176.
26. Weaver, T. E., and J. J. Conkright. 2001. Function of surfactant proteins B and C. *Annu. Rev. Physiol.* 63:555–578.
27. Cruz, A., C. Casals, I. Plasencia, D. Marsh, and J. Pérez -Gil. 1998. Depth profiles of pulmonary surfactant protein B in phosphatidylcholine bilayers, studied by fluorescence and electron spin resonance spectroscopy. *Biochemistry*. 37:9488–9496.
28. Possmayer, F., S.-H. Yu, J. M. Weber, and P. G. R. Harding. 1984. Pulmonary surfactant. *Can. J. Biochem. Cell Biol.* 62:1121–1133.
29. Taneva, S. G., J. Stewart, L. Taylor, and K. M. Keough. 1998. Method of purification affects some interfacial properties of pulmonary surfactant proteins B and C and their mixtures with dipalmitoylphosphatidylcholine. *Biochim. Biophys. Acta*. 1370:138–150.
30. Haagsman, H. P., S. Hawgood, T. Sargeant, D. Buckley, R. T. White, K. Drickamer, and B. J. Benson. 1987. The major lung surfactant protein, SP 28–36, is a calcium-dependent, carbohydrate-binding protein. *J. Biol. Chem.* 262:13877–13880.
31. Bourdos, N., F. Kollmer, A. Benninghoven, M. Ross, and H.-J. Galla. 2000. Analysis of lung surfactant model systems with time-of-flight secondary ion mass spectrometry. *Biophys. J.* 79:357–369.
32. Ross, M., S. Krol, A. Janshoff, and H.-J. Galla. 2002. Kinetics of phospholipid insertion into monolayers containing the lung surfactant proteins SP-B or SP-C. *Eur. Biophys. J.* 31:52–61.
33. Biesinger, M. C., P. Y. Paepegaey, N. S. McIntyre, R. R. Harbottle, and N. O. Petersen. 2002. Principal component analysis of organic monolayers. *Anal. Chem.* 74:5711–5716.
34. Möhwald, H. 1990. Phospholipid and phospholipid-protein monolayers at the air/water interface. *Annu. Rev. Phys. Chem.* 74:441–476.
35. Tocanne, J.-F., and J. Teissie. 1990. Ionization of phospholipids and phospholipid-supported interfacial lateral diffusion of protons in membrane model systems. *Biochim. Biophys. Acta*. 1031:111–142.
36. Sacre, M. M., and J. F. Tocanne. 1977. Importance of glycerol and fatty acid residues on the ionic properties of phosphatidylglycerols at the air-water-interface. *Chem. Phys. Lipids*. 18:334–354.
37. Maltseva, E., V. L. Shapovalov, H. Möhwald, and G. Brezesinski. 2006. Ionization state and structure of L-1,2-dipalmitoylphosphatidylglycerol monolayers at the liquid/air interface. *J. Phys. Chem. B*. 110:919–926.
38. Dicko, A., H. Bourque, and M. Pezolet. 1998. Study by infrared spectroscopy of the conformation of dipalmitoylphosphatidylglycerol monolayers at the air-water interface and transferred on solid substrates. *Chem. Phys. Lipids*. 96:125–139.
39. Blume, A., W. Hubner, and G. Messner. 1988. Fourier transform infrared spectroscopy of $^{13}C{=}O$-labeled phospholipids hydrogen bonding to carbonyl groups. *Biochemistry*. 27:8239–8249.
40. McConnell, H. M. 1990. Harmonic shape transitions in lipid monolayer domains. *J. Phys. Chem.* 94:4728–4731.
41. Vanderlick, T. K., and H. Möhwald. 1990. Mode selection and shape transitions of phospholipid monolayer domains. *J. Phys. Chem.* 94: 886–890.
42. Lee, K. Y. C., M. M. Lipp, J. A. Zasadzinski, and A. J. Waring. 1998. Direct observation of phase and morphology changes induced by lung surfactant protein SP-B in lipid monolayers via fluorescence, polarized fluorescence, Brewster angle and atomic force microscopies. *Proc. Soc Photo. Opt. Instrum. Eng.* 3273:115–133.
43. Benninghoven, A., F. G. Ruedenauer, and H. W. Werner. 1987. Secondary ion mass spectrometry (SIMS). John Wiley & Sons, New York.
44. Hagenhoff, B. 2000. High resolution surface analysis by TOF-SIMS. *Mikrochim. Acta*. 132:259–271.